Topological singularities in cortical orientation maps: the sign theorem correctly predicts orientation column patterns in primate striate cortex

Doron Tal & Eric L. Schwartz

Department of Cognitive and Neural Systems, Boston University, 677 Beacon St. Boston, MA 02215, USA

Optical imaging methods have revealed the spatial arrangement of orientation columns across striate cortex, usually summarized in terms of two measurements at each cortical location: (i) a "best" stimulus *orientation*, corresponding to the stimulus orientation that elicits a maximal response , and (ii), the *magnitude* of the response to the best orientation. This mapping has been described as continuous except at a set of singular points (also termed "vortices" [1] or "pinwheels" [2]). Although prior work has shown that vortex patterns qualitatively similar to the ones observed in visual area 17 of the Macaque cortex can be produced by either band-pass [3] [4] or low-pass [5, 6, 7] filtering of random vector fields, there has been to date little further topological characterization of the structure of cortical vortex patterns. Nevertheless, much theoretical work has been done in other disciplines on mappings analogous to the cortical orientation map. In particular, a recent theorem in the optics literature termed *the sign principle* [8] states that adjacent vortices on zero crossings of a phase (orientation) mapping must always alternate in sign. Using digitized samples of recently published optical recording data in monkey striate cortex [9] we show that the cortical orientation data does indeed possess 100% anti-correlation in vortex sign for next-neighbor vortices, as predicted by the sign theorem.This provides strong experimental support for the assumptions of continuity of cortical vortex maps which underly the sign theorem. Similar analysis predicts a lack of "higher order" vortices in the cortical orientation map, which is also found to be in agreement with optical imaging observations. It also follows from this work that cortical vortices must be created simultaneously in clockwise-anti-clockwise pairs. This suggests a possible basis for a modular (hyper-columnar) relationship among *pairs* of cortical vortices that originate at the same developmental time. In summary, this work indicates that primate visual cortex orientation column structure is best understood in the context of other "ordered continuous media", (e.g. liquid He^3, cholesteric liquid crystals, random optical phase maps, to name only a few) in which an order parameter (orientation in this case) is mapped to a physical space, and in which the topological properties of the mapping determine the observable regularities of the system. We also point out that these methods may well be applied to a variety of other cortical map systems which admit an "order parameter", i.e. for which each cortical position is assigned a continuous stimulus value.

The population response in cortex to oriented stimuli, as measured in optical imaging experiments, is characterized by the following method (e.g. see [4]). The optical response $\rho_i(x,y)$ at each cortical location (x,y) is measured for N different stimulus orientations, θ_i (spanning the entire range of possible orientations, $0^\circ - 180^\circ$). This yields N pairs of values:

$$(\rho_i(x,y),\, \theta_i) \quad (i = 1 \ldots N), \tag{1}$$

where $\rho_i(x,y)$ is the magnitude of the measured response at cortical location (x,y) to a stimulus with orientation θ_i (the angle θ_i is multiplied by two to give a range $[0, 2\pi]$) [1]. The N pairs of measurements ρ_i, θ_i in Eqn. 1 are then combined into an orientation response function [4] $(\rho(x,y),\, \theta(x,y))$, by (i) considering each pair in Eqn. 1 to represent the complex number

$$\rho_i(x,y) e^{\theta_i(x,y)}, \tag{2}$$

and (ii) summing, at each (x,y), the real and imaginary parts of the complex number (Eqn. 2), separately, for each of the N pairs (the result of this stage of processing for optical imaging data from the macaque striate cortex is shown in Fig. 1),

$$\begin{aligned} f_{\mathrm{Re}}(x,y) &= \sum_{i=1}^{N} \rho_i(x,y) \cos\left[\theta_i(x,y)\right] \\ f_{\mathrm{Im}}(x,y) &= \sum_{i=1}^{N} \rho_i(x,y) \sin\left[\theta_i(x,y)\right], \end{aligned} \tag{3}$$

and (iii) converting the real/imaginary representation of Eqn 3 back to a polar representation, using the transformation

$$(\rho(x,y),\, \theta(x,y)) = \left(\sqrt{f_{\mathrm{Re}}(x,y)^2 + f_{\mathrm{Im}}(x,y)^2},\ \arctan \frac{f_{\mathrm{Im}}(x,y)}{f_{\mathrm{Re}}(x,y)} \right). \tag{4}$$

The orientation response function of Eqn. 4 has been used to represent the output of optical recordings of orientation selectivity in striate cortex (e.g., see [9]), in which $\theta(x,y)$ is interpreted as the stimulus

[1] Cortical orientation, considered as an angle, takes values in the range $[0, \pi]$. In the work of Blasdel and his collaborators, the cortical orientation is multiplied by a factor of two, taking values in $[0, 2\pi]$, in order to enforce the circularity of the order parameter space. Both orientation and direction mappings are topologically equivalent, however, and the arguments in this work apply equally to both, since the unit circle S^1, corresponding to the range $[0, 2\pi]$ is topologically equivalent to P^1 (one dimensional projective space) corresponding to the range $[0, \pi]$. This equivalence follows immediately from the existence of a homeomorphism connecting them, namely multiplication by 2.

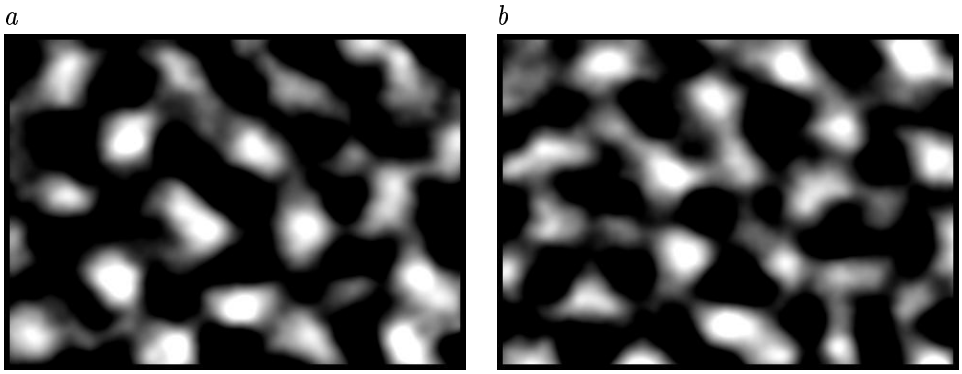

FIG. 1. Complex variable representations of optical imaging data from macaque striate cortex, obtained by processing raw data in the form of Eqn. 1, using Eqn. 3. The raw data are obtained by digitally scanning eight frames each corresponding to a different orientation, θ_i in Eqn. 1 ($\theta_1 = 0°, \theta_2 = 45°, \theta_3 = 90°, \theta_4 = 135°, \theta_5 = 180°, \theta_6 = 225°, \theta_7 = 270°, \theta_8 = 315°$), from Fig. 5 of [9] (used with the author's permission). The frames shown are 3×4mm in size; brighter gray levels indicate positive ranges for f_{Re} and f_{Im} while black regions indicate negative ranges. A polar representation of this data is shown in Fig. 2, and the zero crossings of f_{Re} and f_{Im} are shown in Fig. 4.

orientation that best elicits a response at cortical location (x, y) and $\rho(x, y)$ corresponds to the absolute magnitude of that response. The cortical position variables (x, y) will henceforth be dropped for brevity. The reconstructed $(\rho,\ \theta)$representation (Eqn. 4) of optical imaging data from the macaque striate cortex [9] [2] is shown in Fig. 2.

Optical imaging methods have indicated a dramatic pattern of orientation singularities to exist in primate and cat V-1 [1, 2] (see Fig. 2). The terms "vortices" [10, 4], "pinwheels" [2], "dislocations" [11], "singularities", "orientation singularities" and "phase singularities" [8] have been used interchangeably to refer to singular points of an orientation mapping, around which the entire range of possible orientations $(0° - 180°)$ is continuously represented. All possible orientations are represented in the vicinity of a singularity, allowing for easy visualization of singularities in gray-scale coded orientation maps (Fig. 2a) .

The characteristic feature of the V-1 orientation response function (Eqn. 4) is the existence of local spatial correlation in the orientation response. This spatial correlation of orientation was originally

[2] We thank Dr. Gary Blasdel for generously making the data used in this paper available to us in digital form.

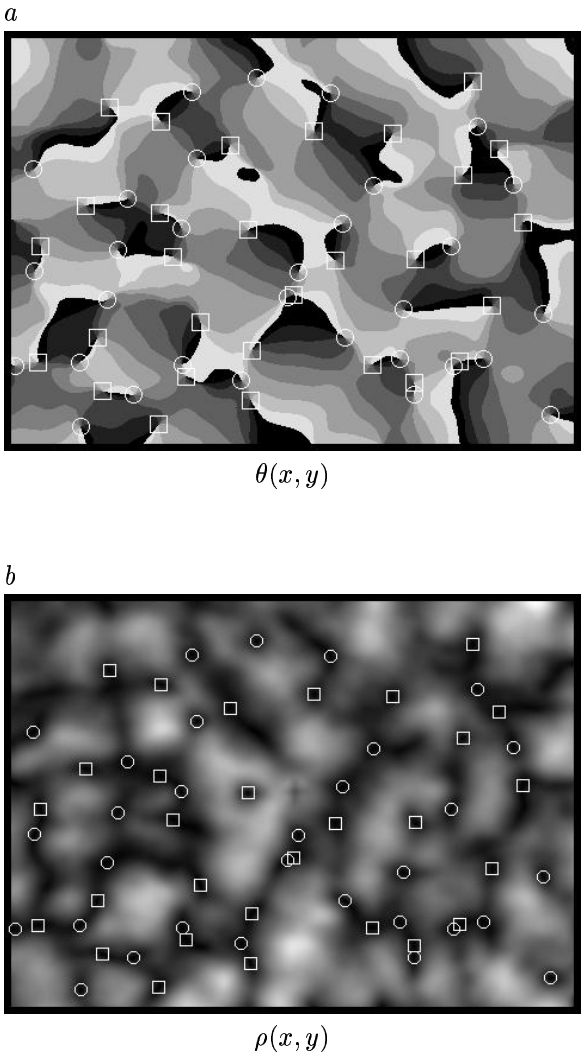

FIG. 2. (ρ, θ) representation of optical imaging data [9], obtained by using the transformation to polar coordinates (Eqn. 4) of the data shown in Fig. 1. (a) The cortical orientation response, showing "best" orientation response at each cortical location. Neighboring gray values correspond to neighboring orientation, with white = black = 0°. Only eight gray-scale values are used for better visualization (thus the banded appearance, which would appear continuous if more gray-scale values were used). (b) The corresponding amplitude map of the orientation response, showing at each cortical location the absolute magnitude of the response to the corresponding best orientation in (a). In both (a) and (b) an automatic vortex detection algorithm was used to superimpose markers denoting vortex signs and locations. Positive (clockwise) vortices are shown as squares, while negative (counterclockwise) vortices are shown as circles. One can verify the properties of singularities in both frames by noticing that in $\theta(x, y)$ (a) all orientations surround each vortex and that vortices appear at the local minima of $\rho(x, y)$ (b).

termed "sequence regularity" [12]: nearby neurons or locations in cortex are characterized by nearby values of best orientation response. The modification to this statement, as a result of optical imaging, has been the observation of singular points around which all orientations are locally represented.

There are a wide range of analogies in the physics of continuous media to the striate cortical vortex pattern shown in Fig. 2 (see [13] for a review): vortex patterns in liquid Helium[3], cholesteric liquid crystals and random optical phase fields [14], to name just a few analogies [3]. All of these systems, as well as striate cortex, are best understood in terms of the topological consequences of assigning an "order parameter" (in this case, the orientation response in cortex, represented as an angle) to each point of some underlying physical space (in this case, imaged "pixels" of the two-dimensional cortical sheet). The order parameter describing orientation, namely angle, may be viewed in topological terms as the boundary of the unit circle S^1, in the sense that points in S^1 are in one-to-one correspondence with possible orientations. S^1 is not simply connected [4]. The cortical plane, however, is topologically modeled as a subset of R^2, the two-dimensional real number manifold, which *is* simply connected. Cortical orientation maps therefore are instances of the mapping $S^1 \rightarrow R^2$, between spaces of different connectivity (*i.e.*, different homotopy classes [13]). A continuous mapping between spaces of different connectivity *must* contain singularities such as the vortices observed in cortex [13], as has been previously discussed [7] and recently observed in optical recording experiments (Fig. 2). In prior work, it has been demonstrated that random orientation maps, when spatially filtered either by a band-pass [17, 3] or a low-pass [7] filter, provide similar vortex maps to those observed in optical recording. These methods of generating vortex maps all rely on the filter's introduction of local correlation (and thus, "continuity") in the mapping and on the fact that the mapping is between spaces of different connectivity, to produce vortex patterns. These same spatial filter methods have been applied more recently for constructing random vortex models of cortical orientation [18, 19].

[3]The relationship of the cortical orientation pattern to vortex patterns in fluid mechanics was first noted in [10], and the analogy to patterns of phase disorder, as in cholesteric liquid crystals was discussed in [15]. The suggestion that cortical orientation maps are a phase singularity pattern has also been previously suggested [16]. The relationship of cortical orientation to filtered patterns of spatial orientation noise was first discussed in [3].

[4]A simply connected space is one in which all closed curves may be smoothly shrunk to a point.

Mathematically, a vortex is characterized by two key properties of the orientation mapping $\theta(x, y)$ and the amplitude mapping $\rho(x, y)$. First, all orientations are represented, at least once, around the singularity center. Equivalently, the contour integral along any loop in $\theta(x, y)$ that surrounds a (single) vortex is always an integral number of 2π radians. This follows from the presumed continuity and single-valuedness of the cortical mapping everywhere except at the singularity itself. Since the mapping is continuous, when traversing a loop surrounding a vortex from starting point (x_0, y_0) eventually returning to (x_0, y_0), one must also return along the corresponding path in orientation space to the angle θ_0 that was mapped onto (x_0, y_0). The return to the same angle can only happen in two ways, either (a) the entire orientation mapping is (uninterestingly) constant or (b) as the loop in cortex is traversed, the underlying orientations encountered also form a loop in orientation space of 0,1,2,...n "windings". It turns out that a singularity must occur inside the loop when case (b) above is satisfied for $n \geq 1$ [13]. In this case, the sum of angle differences along a loop surrounding a singularity, as it is traversed in a clockwise direction, is an integer multiple of 2π radians. This integer, which can be positive or negative (corresponding to a positive or negative increase in angle along a clockwise traversal of the loop, respectively) is termed the *winding number*. In summary, a singularity exists if and only if its winding number is nonzero. The *sign* of a vortex is defined as the sign of its winding number.

In the amplitude mapping, $\rho(x, y)$, a singularity is characterized by the amplitude of the response function approaching zero in the vicinity of the vortex center and equaling zero at the center. The amplitude mapping at singularities in a *discrete* medium (such as a video image obtained by the optical imaging method) may differ slightly from zero due to discretization (both the underlying neuronal system and its digital optical image are discrete). Nevertheless, singularities in discrete mappings always occur at *local minima* of the mapping, in our experience, as expected (and explained) by the continuum arguments summarized above, and in the literature of ordered media [13].

The main result of the present paper is that a theorem developed in the context of random optical wave fields [8] termed the *sign principle* accurately characterizes the primate V-1 orientation map. The

sign principle states that adjacent singularities must always alternate in sign along any zero crossing path of the real (f_{Re}) or the imaginary (f_{Im}) representation of an orientation map. Fig. 3 illustrates the proof of the sign principle (based on the proof in [8]). Fig. 4 demonstrates that the sign-principle correctly predicts the structure of primate V-1 orientation maps measured by optical imaging [9] [5].

This paper places studies of cortical neuroanatomy into the well developed context of continuous media, which is quite distinct from the "neural network" point of view where the discrete nature of neural structure is emphasized. This "supra-neuronal" [20] level of description of cortical architecture is supported by the validity of the sign principle in accurately characterizing the cortical orientation map. Specifically, a wide range of phenomena related to cortical orientation map structure is clarified by the use of the sign principle. These will now be briefly outlined.

The real and imaginary zero crossings of the observed orientation map provide a natural coordinate system for analyzing the V-1 orientation map. For example, the pattern statistics of the vortex map (e.g. the probability of neighboring vortices being of opposite sign), appears to be a random variable when analyzed in spatial (i.e. conventional Eucledian) metric but appears to be rigorously correct when the metric is computed along zero crossing lines, as per the sign principle. Further statistical characterization of cortical orientation structure is likely best done by taking this coordinate system into account [6]

As seen in this paper, winding number characterizes the local structure of cortical "vortices". "Winding number" has been termed "topological charge", since it obeys a form of conservation law which is similar to that of conventional (electro-magnetic) charge conservation [22]. Briefly, vortices are created and destroyed in "pairs", as we have frequently observed in computer simulation. The sign

[5] In order to produce Fig. 4, and for further analysis that takes into consideration vortex locations, we have developed and empirically evaluated an accurate vortex detection algorithm. The main steps of the algorithm consist of (i) finding all pixels in the image whose amplitude is smaller than the amplitude of all 8 nearest neighbor pixels; (ii) integrating the angle-differences along a traversal of the 8 nearest neighbor pixels and along a slightly larger circle (radius = 2 pixels) centered on each pixel, in order to compute the winding number (and thus also the vortex sign) and ensure that the winding number is close to an integral multiple of 2π radians. All vortices in Figs. 1, 2 and 4 were automatically detected using this algorithm, which produced no errors (as verified by visual checking) for the orientation map used in this analysis and for other experimental and computer generated orientation maps.

[6] There is a high degree of nearest neighbor correlation in natural vortex patterns. Statistical studies using the Eucledian metric have shown 85-90% anti-correlation in sign among vortices in optical interferometry experiments [8] and later the same anti-correlation percentages were computed for vortices in optical imaging data [21].

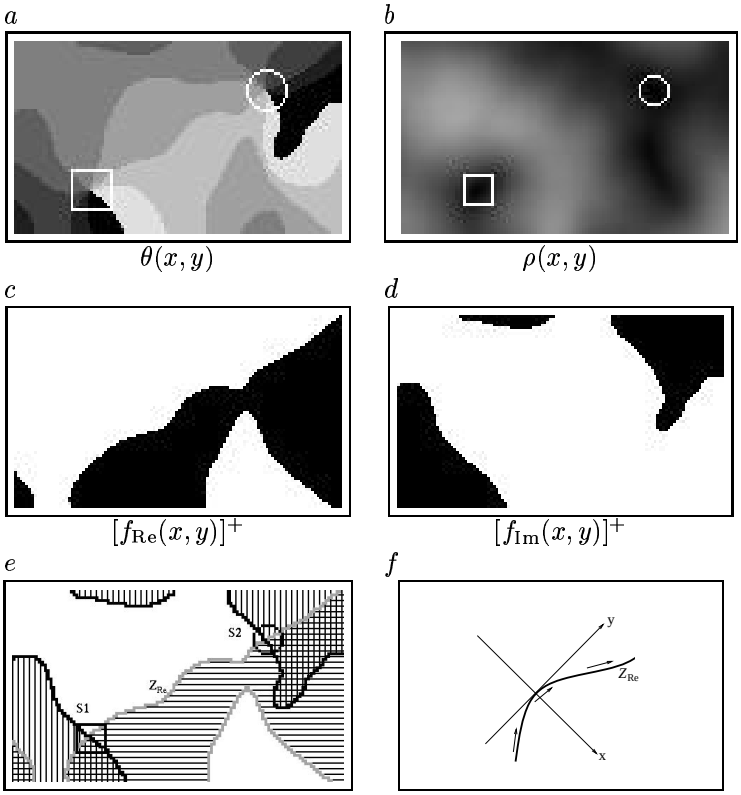

Figure 3. Proof of the sign principle, assuming a particular choice of zero crossing structure for illustrative purposes. The sign principle states that adjacent vortices on any zero crossing path Z_{Re} (Z_{Im}) of the real (imaginary) representation, f_{Re} (f_{Im}), of Eqn. 3 must alternate in sign, where the vortex "sign" is positive if the direction of increase in orientations around the vortex is clockwise, and negative if it is counterclockwise. (a-f) A section of the cortical orientation map (Fig. 2), used to demonstrate the proof of sign principle. (a) Cortical orientation preference denoting the orientation that elicits a best response at each cortical location. (b) Magnitude of the orientation response in (a), showing expected local minima at vortex centers. (c-d) Real/imaginary representation of the mapping in (a,b), obtained according to Eqn. 3, and thresholded at zero, positive regions are black. (e) The zero crossings of the mappings in (c) and (d), superimposed. Gray lines: the zero crossing paths of f_{Re}; black lines: the zero crossing paths of f_{Im}; horizontal- line shading: regions in which $f_{\mathrm{Re}} > 0$; vertical-line shading: regions where $f_{\mathrm{Im}} > 0$; S1 and S2 denote the locations of two singularities in this mapping. (f) A schematic of the mapping near the singularity S1 in (e) showing the coordinate system used at each singularity in the sign principle proof below. To prove the sign principle we imagine walking along Z_{Re} from S1 to S2. At each point (x_i, y_i) on Z_{Re} we use the coordinate system whose origin is (x_i, y_i), y-axis is parallel to the tangent of Z_{Re} at (x_i, y_i), x-axis is orthogonal to the y-axis and the positive part of the x-axis is aligned with the positive part of f_{Re}, as shown in (f). It can be shown [11] that the sign of a vortex is given by the sign of $\begin{vmatrix} \frac{\partial f_{\mathrm{Re}}}{\partial x} & \frac{\partial f_{\mathrm{Re}}}{\partial y} \\ \frac{\partial f_{\mathrm{Im}}}{\partial x} & \frac{\partial f_{\mathrm{Im}}}{\partial y} \end{vmatrix} = \frac{\partial f_{\mathrm{Re}}}{\partial x}\frac{\partial f_{\mathrm{Im}}}{\partial y} - \frac{\partial f_{\mathrm{Re}}}{\partial y}\frac{\partial f_{\mathrm{Im}}}{\partial x}$. In the chosen coordinate system, $\frac{\partial f_{\mathrm{Re}}}{\partial y}$ is always zero because the y-axis is always tangent to Z_{Re}. Moreover, as we move along Z_{Re} from S1 to S2, $\frac{\partial f_{\mathrm{Re}}}{\partial x}$ is always positive since (by our initial assumption) f_{Re} always increases to our right and decreases to our left. Thus, the sign of a singularity encountered along our path is solely dependent on the sign of $\frac{\partial f_{\mathrm{Im}}}{\partial y}$. At S1, $\frac{\partial f_{\mathrm{Im}}}{\partial y} < 0$ (because f_{Im} increases in the direction pointing from S1 to S2, opposite to the increasing direction of the y-axis), implying that S1 is a negative vortex. Since f_{Im} is positive between S1 and S2 and since f_{Im} must *decrease* back to zero at S2 (because singularities occur only at the intersections of zero crossings), at S2 $\frac{\partial f_{\mathrm{Im}}}{\partial y} > 0$ and thus S2 must have an opposite sign to S1. By symmetry, the same proof applies to traversal of Z_{Im} and for the other possible directions of increase of f_{Re} and f_{Im} at S1.

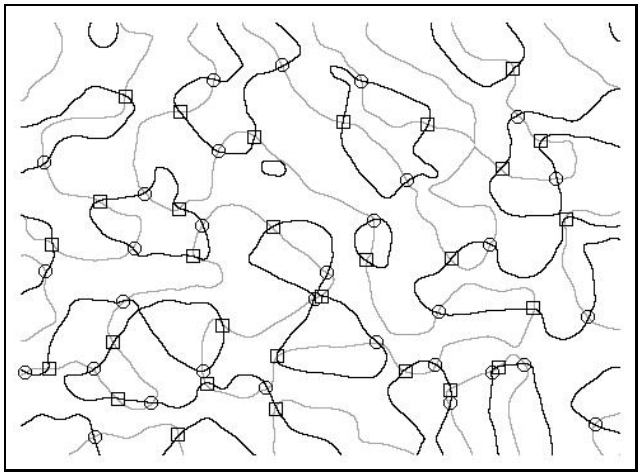

FIG. 4. Demonstration that the sign principle holds for a previously published cortical orientation map, reconstructed from the data [9] shown in Figs. 1 and 2. Gray lines denote the zero crossings Z_{Re} of f_{Re} in Fig. 1 while black lines correspond to Z_{Im}. Vortices occur only at the intersections of zero crossings Z_{Re} and Z_{Im}. The vortex locations and signs are shown by either squares or circles, corresponding to positive or negative signs, respectively. Adjacent vortices on any zero crossing path always alternate in sign, as predicted by the sign principle.

principle shows why this is the case: vortices are created when a real [resp. imaginary] zero crossing curve "wanders" across an imaginary [resp. real] one. Generically, two vortices (of opposite sign) will be produced simultaneously by this mechanism, since the zero crossing lines are generically closed and therefore intersections come in pairs [7]. The same argument in reverse describes vortex "annihilation", caused for example by smoothing or averaging. Thus, if one low-pass filters a random orientation map, the low-pass filter causes nearby positive and negative vortices to be "annihilated", i.e. to disappear, leaving a singularity free region, as shown in [7]. The sign principle thus provides deep insight into the appearance or disappearance of vortex pairs. Moreover, as has been noted before [7], any form of spatial filtering (either low pass or band-pass) is capable of producing new vortices or annihilating existing vortices. Therefore, care must be observed in digital manipulation of optical recording data, especially because (somewhat counter-intuitively) a "blurring" operation such as low pass filtering can actually produce extremely "sharp", yet artifactual, vortex structure.

Winding numbers greater than 1 have not been observed in V-1 optical recordings. This can be

[7] This statement can be violated by a situation of tangency between the real and imaginary zero crossing, but this situation is topologically unstable, i.e. collapses into the pair-creation mechanism under a small perturbation.

understood with reference to the pair-creation mechanism, occurring when two zero crossing paths have intersected. Higher order vortices require more than two zero crossing lines to intersect at a point. Aside from being statistically unlikely, this situation is also topologically unstable, since it degenerates under infinitesimal perturbation into distinct first order vortex pairs.

Vortices are created in pairs of positive-negative winding number. This provides a natural identification of neighboring cortical singularities, identifying those pairs of adjacent vortices (in the zero crossing metric) which were created at a single zero crossing intersection event, i.e. adjacent singularities along a zero crossing path that were created simultaneously in a vortex pair creation. In practice, there appears to be no way to create this labeling after the fact, but it could be done in principle by following developmental trajectories. Moreover, this identification of cortical vortex pairs seems to provide a solution to the long existing question of whether there is a modular supra-columnar (i.e. hypercolumn like) pattern in V-1, as originally suggested by Hubel and Weisel [12]. Since cortical vortex pairs must be created simultaneously, via intersection of two zero crossing contours, there is a natural pair-wise identification of nearby vortices which can be interpreted as providing a basis for a "hypercolumn" like pairing of singularities.

Finally, it is important to note that the entire analysis provided here, in terms of the topological properties of ordered media, is likely to carry over to other cortical feature maps. For example, the direction column structure of MT cortex [23] is also a map of $S^1 \to R^2$, and thus would be expected to provide similar supra-neuronal behavior as outlined above for the V-1 orientation column map. Further, cortical feature maps can be described in terms of the same language used here, i.e. the assignment of an order parameter (i.e. the feature space) to a physical space (i.e. the cortex). The topological properties of these two spaces are then expected to determine the qualitative structure of arbitrary cortical feature maps in the manner which has already been well characterized in the context of the topological defects of ordered media [13]. Thus, supra-neuronal architectures in cortex may be, in addition to being accessible to experimental techniques such as optical recording, accessible to a well developed body of theoretical methodology.

ACNKOWLEDGEMENTS. We Thank Dr. Gary Blasdel for his contribution of raw optical imaging data.

CORRESPONDANCE should be sent to E.L. Schwartz (email: eric@thing4.bu.edu). This work supported by grants NIMH 5R01MH45969 and ONR N00014-95-1-0409.

References

[1] Blasdel, G. and Salama, G. *Nature* **321**, 579–585 (1986).

[2] Bonhoeffer, T. and Grinvald, A. *Nature* **353**, 429–431 (1991).

[3] Rojer, A. and Schwartz, E. L. *Biological Cybernetics* **62**, 381–391 (1990).

[4] Blasdel, G. *Abstracts, Society for Neuroscience* **17**, 1088 (1991).

[5] Schwartz, E. L. and Rojer, A. S. Technical Report 593, Courant Institute of Mathematical Sciences, 251 Mercer Street, May (1991).

[6] Schwartz, E. L. and Rojer, A. S. *Society for Neuroscience Abstracts* **18**, 742 (1992).

[7] Schwartz, E. and Rojer, A. In *ICPR Proceedings*, ICPR-12. International Conference on Pattern Recognition, 150–155 (1994).

[8] Shvartsman, N. and Freund, I. *J. Opt. Soc. Am. A* **111**(10), 2710–2718 (1994).

[9] Blasdel, G. G. *Journal of Neuroscience* **12**(8), 3139–3161 August (1992).

[10] Schwartz, E. L. *Biological Cybernetics* **28**, 1–24 (1977).

[11] Nye, J. F. and Berry, M. V. *Proc. R. Soc. Lond. A* **336**, 165–190 (1974).

[12] Hubel, D. H. and Wiesel, T. N. *J. Comp. Neurol.* **158**, 267–293 (1974).

[13] Mermin, N. D. *Rev. Modern Physics* **51**, 591–648 (1979).

[14] Shvartsman, N. and Freund, I. *Physical Review Letters* **72**(7), 1008–1011 (1994).

[15] Schwartz, E. L. *Biological Cybernetics* **37**, 63–76 (1980).

[16] Winfree, A. T. *When Time Breaks Down.* Princeton University Press, Princeton N.J., (1987).

[17] Rojer, A. and Schwartz, E. L. *IJCNN Proceedings* **II**, 603–613 (1989).

[18] Blasdel, G., Obermayer, K., and Kiorpes, L. *Vis. Neurosci.* **12**, 589–603 (1995).

[19] Grossberg, S. and Olson, S. J. *Neural Networks* **??**, 883–894 (1994).

[20] Schwartz, E. L., ed. *Computational Neuroscience.* MIT Press, Cambridge, MA, (1990).

[21] Tal, D. and Schwartz, E. L. *ARVO presentation abstract – In Press* (), () (1996).

[22] Finkelstein, D. *Annals of Physics* **6**, 230–243 (1959).

[23] Albright, T. D. *J. Neurophysiology* **52**, 1106–30 (1984).